Fitoterapia 100 (2015) 174–178

Contents lists available at ScienceDirect

Fitoterapia

journal homepage: www.elsevier.com/locate/fitote

Molecular mechanism of tanshinone IIA and cryptotanshinone in platelet anti-aggregating effects: an integrated study of pharmacology and computational analysis

Francesco Maione [a], Vincenza Cantone [b], Maria Giovanna Chini [b], Vincenzo De Feo [b], Nicola Mascolo [a,*], Giuseppe Bifulco [b,**]

[a] Department of Pharmacy, University of Naples Federico II, Via Domenico Montesano 49, 80131 Naples, Italy
[b] Department of Pharmacy, University of Salerno, Via Giovanni Paolo II 132, 84084 Fisciano, SA, Italy

ARTICLE INFO

Article history:
Received 6 November 2014
Accepted in revised form 27 November 2014
Available online 10 December 2014

Keywords:
Salvia miltiorrhiza Bunge
Tanshinones
Docking study
Platelet aggregation
P2Y receptors

ABSTRACT

Tanshinone IIA and cryptotanshinone are two pharmacologically active diterpenoids extracted from the roots of *Salvia milthiorriza* Bunge, a plant used in Chinese traditional medicine for the treatment of some cardiovascular and cerebrovascular disease. Until now, the molecular mechanisms of action of these two diterpenoids on platelets are partially known. To clarify this aspect, here we utilized an integrated study of pharmacology and computational analysis.
Our results demonstrate that cryptotanshinone is able to inhibit in a concentration dependent manner the rat platelet aggregation and also is endowed of G_i-coupled $P2Y_{12}$ receptor antagonist as demonstrated by docking studies. This computational method was also performed for tanshinone IIA demonstrating even for this diterpenoid an interaction with the same receptor.
The findings from our study enable a better understanding of tanshinone IIA and cryptotanshinone biological properties, which could ultimately lead to the development of novel pharmaceutical strategies for the treatment and/or prevention of some cardiovascular disease.

1. Introduction

It is well known that adenosine diphosphate (ADP) plays a key role in platelet activation. Aberrant activation of platelets by pathological factors is commonly associated with vascular disease and thrombosis [1]. ADP activates platelets through two G-protein coupled receptors, the G_q-coupled $P2Y_1$ receptor and G_i-coupled $P2Y_{12}$ receptor [2]. These receptors are targets for common anti-platelet agents such as aspirin and clopidogrel [3]. However, the chronic use of these agents is limited because they can induce resistance or adverse effects on gastrointestinal tract [4] and, as often happens, drug toxicity may be increased when multiple antiplatelet drugs are used. In this context, new antiplatelet agents are greatly needed to increase the efficacy and reduce side effects. Nowadays, an increasing number of studies have been performed to search new agents from natural source and it is well know that some phytochemicals from plants have generated new drugs [5–7].

Tanshinone IIA (TIIA, **1** in Fig. 1), from roots of *Salvia milthiorriza* Bunge (Lamiaceae) (also known as danshen), is an example of diterpenoid, studied *in vitro* and *in vivo*, able to inhibit platelet aggregation and to induce an increase of blood viscosity. We have previously demonstrated that these effects are mediated *via* the modulation of tubulin acetylation and inhibition of Erk-2 phosphorylation [8]. In our continuing studies on pharmacology of danshen constituents, here we explored the effect of cryptotanshinone (CRY, **2** in Fig. 1), another major lipophilic constituent present in danshen, on platelet aggregation [9–11].

* Corresponding author. Tel.: +39 081678412; fax: +39 081678403.
** Corresponding author. Tel.: +39 089969741; fax: +39 089969602.
E-mail addresses: nmascolo@unina.it (N. Mascolo), bifulco@unisa.it (G. Bifulco).

http://dx.doi.org/10.1016/j.fitote.2014.11.024
0367-326X/

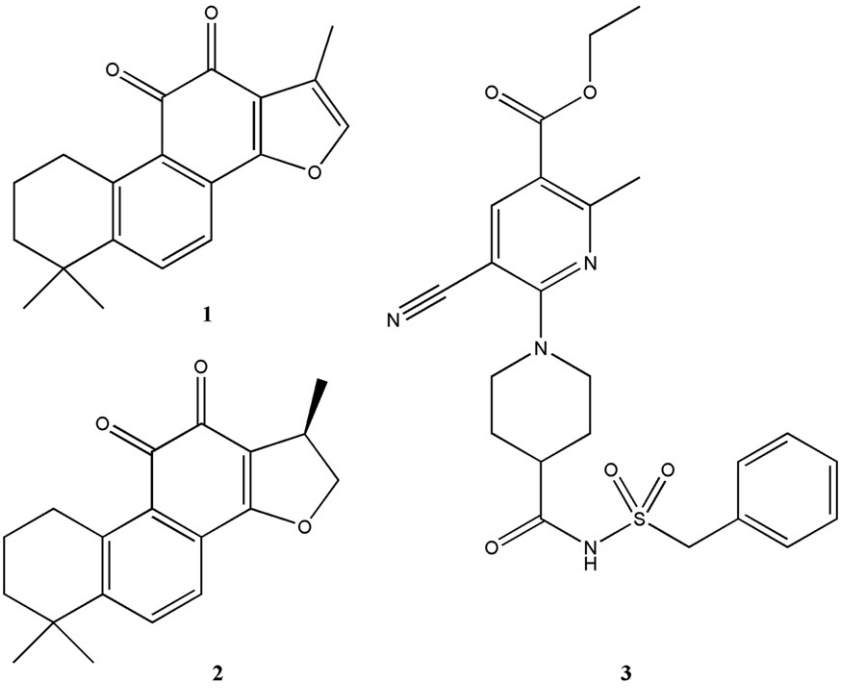

Fig. 1. Molecular structure of tanshinone IIA (**1**), cryptotanshinone (**2**) and AZD1283 (**3**).

To this aim, we have tested *in vitro* the potential antiaggregant effect of **2** and simultaneously the interaction of **1** and **2** on the purinergic platelet receptor by a computational analysis.

2. Results and discussion

Tanshinone IIA (**1**), one of the lipophilic constituents present in danshen, is able to inhibit platelet aggregation and to induce an increase of blood viscosity *via* the modulation of tubulin acetylation and inhibition of Erk-2 phosphorylation [8]. Here, we expand our previous observations and, by a molecular docking study, we investigated the interaction of **1** with the binding site of G-protein-coupled purinergic receptors $P2Y_{12}R$ (PDB code: 4NTJ) [12] using AutodockVina software [13]. $P2Y_{12}R$, is a target for the development of novel anti-platelet therapies being involved in the regulation of the platelet activation and thrombus formation [14,15]. In particular, in order to rationalize the binding mode of **1**, we have used the crystal structure of $P2Y_{12}R$ in complex with ethyl 6-(4-((benzysulphonyl)carbamoyl)piperidin-l-yl)-5-cyano-2-methylnicotinate non-nucleotide antagonist (AZD1283, **3** in Fig. 1) [12] as model receptor for our docking studies.

As already reported [12], **3**, a potent antagonist of the $P2Y_{12}$, makes a number of polar and hydrophobic contacts in the pocket 1 with side chains of amino-acids of the helices III–VII, mainly interacting with TYR105, PHE252, ARG256, TYR259, LEU276 and LYS280 (Fig. 2), and adopting a different orientation with respect to the agonist [16]. On this basis, we have analyzed the binding mode of **1** in the $P2Y_{12}R$ in comparison with the co-crystallized antagonist **3**. From the analysis of this docking studies, even if **1** occupies the pocket 1 (helices III, IV and V), in analogy to the **3**, accounting for its antagonist activity, it poorly interacts with helices VI and VII (Fig. 3) due to its smaller size compared to **3** (Figs. 2 and 3).

In more details, **1** shows polar interactions with ASN159, ASN191 and ARG256, and it makes hydrophobic contacts with VAL102, PHE252, ARG256 and LYS280. Furthermore, **1** establishes a weak hydrogen bond between oxygen at position 11 and the side chain of CYS194, and it forms π–π interactions with the side chains of TYR105, as observed for **3**, and of TYR109 (Fig. 3).

In our continuing studies on pharmacology of danshen constituents, here we also explored the effect of **2**, another major lipophilic constituent present in danshen, on platelet aggregation.

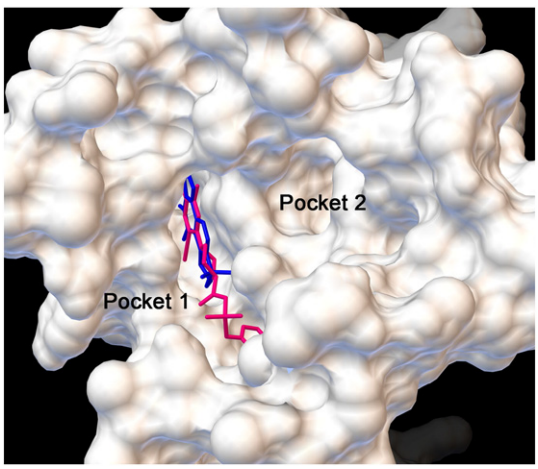

Fig. 2. 3D model of tanshinone IIA (colored by blue sticks) and AZD1283 (colored by fuchsia sticks) in the antagonist binding site of $P2Y_{12}R$ (PDB code: 4NTJ).

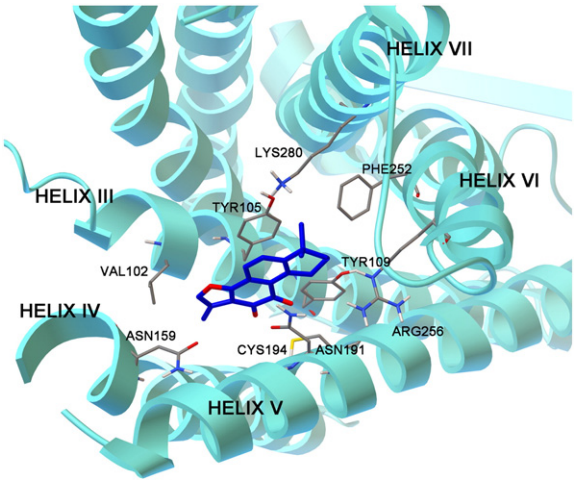

Fig. 3. 3D model of tanshinone IIA (colored by atom types: C blue, O red) into $P2Y_{12}R$ binding site. Residues in the active site (pocket 1) are represented in sticks and balls (colored by atom types: C gray, N blue, O red, H white, S yellow).

Fig. 4 shows a concentration-dependent inhibition of reversible platelet aggregation expressed as % of inhibition of AUC (Fig. 4A) or amplitude (Fig. 4B) induced by **2** (0.5, 5 and 50 μM) added 1 min before the addition of ADP (3 μM). **2** at a concentration of 50 μM displayed the maximum inhibitory activity in terms of inhibition of AUC (66.30 ± 14.11%; $P < 0.01$) and amplitude (31.00 ± 7.09 %; $P < 0.01$).

Moreover, considering the structural similarity of the **2** with **1** and its biological activity reported above, we have performed molecular docking studies of **2** with the $P2Y_{12}R$ receptor (Fig. 5). Cryptotanshinone shows the same polar interactions and hydrophobic interactions of **1** in the $P2Y_{12}R$ binding site interacting with helices III, IV and V, and it displays an additional hydrophobic interaction with VAL190 (Fig. 6), accounting for the predicted similar energy of binding. The absence of the double bond at position 17 in **2**, in fact, does not affect its binding with $P2Y_{12}R$ with respect to **1**, and according with the biological data, our docking results confirm its antiaggregant activity.

3. Concluding remarks

In conclusion, even if tanshinone IIA and cryptotanshinone show a relatively simple skeleton in comparison to the AZD1283, our docking results suggest that their established interactions with $P2Y_{12}R$ are sufficient to rationalize the $P2Y_{12}R$ antagonist activity of these two diterpenoids. The findings from our study enable a better understanding of **1** and **2** biological properties, which could ultimately lead to the development of novel pharmaceutical strategies for the treatment and/or prevention of some cardiovascular disease.

Furthermore, the tanshinones, such as tanshinone IIA and cryptotanshinone, and their derivatives, in fact, could be utilizable as lead compounds for future cancer and anti-inflammatory active molecules [17], being able to inhibit the growth and proliferation of cancer cells, to induce cell cycle arrest and apoptosis, and to inhibit angiogenesis.

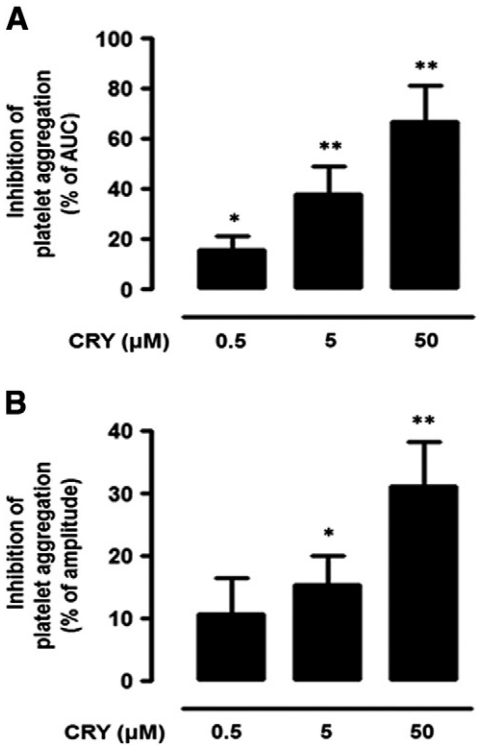

Fig. 4. Concentration dependent effect of cryptotanshinone (**2**) on ADP-induced platelet aggregation. Rat PRP were incubated with **2** (0.5–50 μM) for 1 min, and then exposed to ADP (3 μM) to induce platelet aggregation. Percent (%) inhibition of aggregation was expressed in terms of AUC (**A**) or amplitude (**B**) calculated as the difference between the maximum value of aggregation in presence of ADP plus vehicle and the value obtained in the presence of ADP plus **2**. Data are expressed as mean ± SEM. $^{*}P < 0.05$ vs vehicle; $^{**}P < 0.01$ vs vehicle (one way ANOVA; $n = 7$).

Indeed, tanshinone IIA shows both *in vitro* and *in vivo* biological effects comparable to those of pan-inhibitors, such as curcumin and oridonin, and interestingly, it interferes with the pathway of biosynthesis of PGE_2, in particular with the COX2

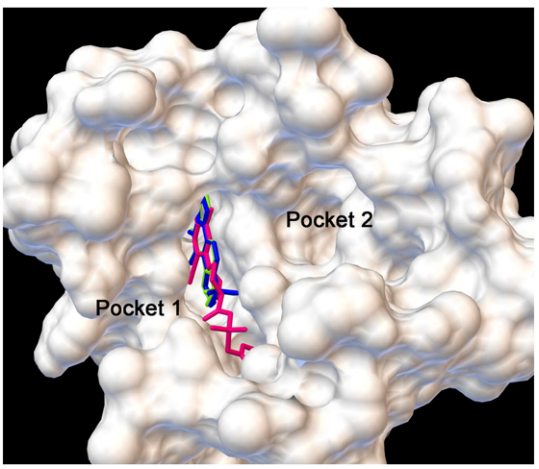

Fig. 5. 3D model of tanshinone IIA (colored by blue sticks), AZD1283 (colored by fuchsia sticks), and tanshinone IIA (colored by blue sticks) into $P2Y_{12}R$ binding site.

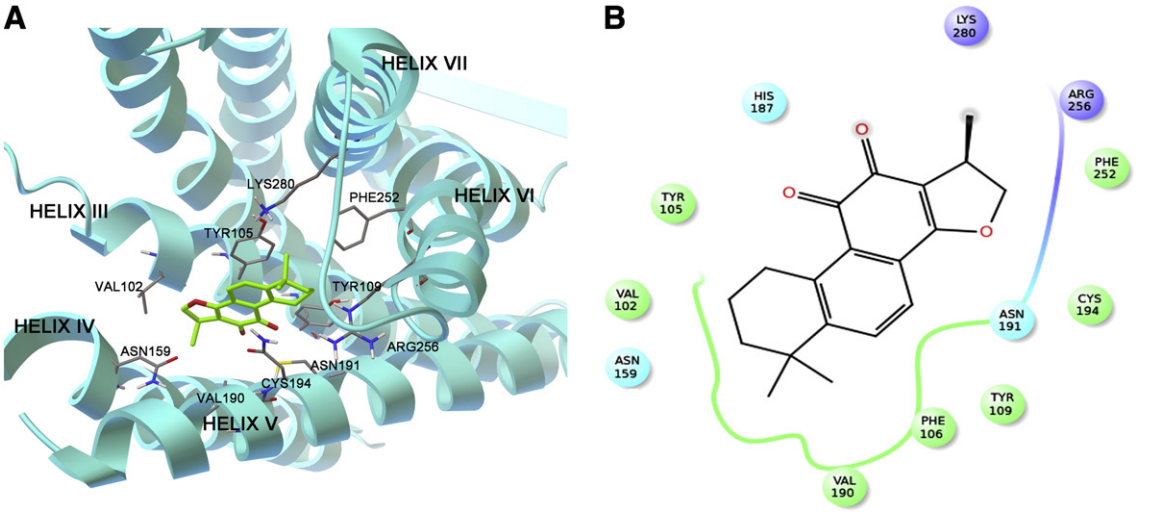

Fig. 6. (**A**) 3D model of cryptotanshinone (colored by atom types: C green, O red) in the binding site of $P2Y_{12}R$. Residues in the active site are represented in sticks and balls (colored by atom types: C gray, N blue, O red, H white). (**B**) 2D panel representing the interactions between cryptotanshinone and residues in $P2Y_{12}R$ binding site (charged residues are colored in violet, polar residues are colored in light blue, and hydrophobic residues are colored in green).

receptor [17,18]. On these bases, here we suggest the possible interaction of **1**, in analogy with **2** (See Supporting Information), with the microsomial prostaglandin E_2 synthase (mPGES-1). The inhibition, in fact, of these two diterpenoids on PGE_2 production by mPGES-1, could suggest a potential association of their anti-inflammatory and antiplatelet activity.

4. Experimental

4.1. Animals

Male Wistar rats (250–300 g; Harlan Nossan, Correzzana, Milan, Italy) were used for all the experiments. Animals were kept under standard conditions, with food and water *ad libitum* and maintained in a 12 h/12 h light/dark cycle at 22 ± 1 °C. All the *in vivo* procedures were in accordance with the Italian legislative decree (D.L.) no. 116 of January 27, 1992 and associates European Community guidelines (EEC Directive of 1986; 86/609/EEC). All efforts were made to minimize animal suffering and to reduce their number.

4.2. Chemicals

Cryptotanshinone (≥97%, HPLC), adenosine diphosphate (ADP) and dimethyl sulfoxide (DMSO) were obtained from Sigma-Aldrich Co. (Milan, Italy). Unless otherwise stated, all the other reagents were from Carlo Erba Reagents (Milan, Italy).

4.3. In vitro platelet aggregation assay

In vitro platelet aggregation was measured according to the turbidimetric method, using two-channel aggregometer (Chrono-Log, Corporation, Mod. 490, USA). Blood anticoagulated with 3.2% sodium citrate (1:9 citrate/blood, *v/v*) was withdrawn from male Wistar rats (anesthetized by enflurane) by cardiac puncture. Platelet-rich plasma (PRP) and platelet-poor plasma (PPP) were prepared as previously described [6,8]. Briefly, PRP was obtained by centrifugation at 800 rpm for 15 min at 25 °C. PPP was prepared from the precipitated fraction of PRP by centrifugation at 2000 rpm for 20 min at 25 °C. PRP was adjusted to 3×10^8 platelets/ml. Next, 250 μl of PRP was incubated at 37 °C for 1 min in the cuvette with 20 μl of **2** solution at a final concentration of 0.5, 5 and 50 μM. **C**ryptotanshinone-vehicle (0.3% DMSO in distilled water) was used as control. After incubation, platelet aggregation was induced by the addition of 20 μl ADP (3 μM). The maximum platelet aggregation rate was recorded within 10 min with continuous stirring at 37 °C. The light transmittance was calibrated with PPP. The percentage (%) of inhibition of platelet aggregation was calculated by the following formula: $[(X - Y)/X] \times 100\%$. *X* was the maximum aggregation rate of vehicle-treated PRP; *Y* was the maximum aggregation rate of sample-treated PRP and was expressed in terms of AUC (% of total response duration from reagent addition).

4.4. Computational methods

The chemical structures of tanshinone IIA and cryptotanshinone were built with Maestro (version 9.6) [19] and processed with LigPrep version 2.8 [19], generating all the possible tautomers, protonation states at a pH of 7.4 ± 1.0; and finally minimized using OPLS 2005 force field. For the subsequent docking calculations, the structures were converted in the .pdbqt format using Autodock Tools 1.5.6, adding Gasteiger charges. The three-dimensional structure of protein target (PDB code: 4NTJ) was prepared with the Schrödinger Protein Preparation Wizard [19]. Protein .pdb file obtained was then processed with Autodock Tools 1.5.6 and converted in .pdbqt format, merging non polar hydrogens and adding Gasteiger charges. Charge deficit was spread over all atoms of related residues. We

chose coordinates and dimensions along x, y, and z axes of the grid related to the site of presumed pharmacological interest. In particular, we chose the binding site between III and VII chains, and a grid box size of 28 × 28 × 28 and centered at 17.036(x), 96.731(y), and 50.379(z) was set, with a spacing of 1.0 Å between the grid points. Molecular docking study of these two compounds on $P2Y_{12}R$ was performed using Autodock Vina [13]. The exhaustiveness value was set to 62, saving 30 conformations as maximum number of binding modes. Autodock Vina results were analyzed with Autodock Tools 1.5.6. Illustrations of the 3D models were generated using Autodock Tools 1.5.6 and Maestro software [19].

4.5. Statistical analysis

All assays were repeated at least in triplicate and the results were expressed as mean ± standard error of mean (SEM). Results were analyzed with one way analysis of variance (ANOVA), followed by Bonferroni's test for multiple comparisons. In some cases, one sample *t*-test was used to evaluate significance against the hypothetical zero value. The analysis was performed using GraphPad Prism Software version 4.0. *P* values less than 0.05 were considered significant.

Acknowledgments

Financial support by Associazione Italiana Ricerca sul Cancro (AIRC) Grant IG_12777—Bifulco Giuseppe.

Appendix A. Supplementary data

Supplementary data to this article can be found online at http://dx.doi.org/10.1016/j.fitote.2014.11.024.

References

[1] Davi G, Patrono C. N Engl J Med 2007;357:2482–94.
[2] Kahner BN, Shankar H, Murugappan S, Prasad GL, Kunapuli SP. J Thromb Haemost 2006;4:2317–26.
[3] Gaglia MAJr, Manoukian SV, Waksman P. Am Heart J 2010;160:595–604.
[4] Angiolillo DJ, Fernandez-Ortiz A, Bernardo E, Alfonso F, Macaya C, Bass TA, et al. J Am Coll Cardiol 2007;49:1505–16.
[5] Bonito MC, Cicala C, Marcotullio MC, Maione F, Mascolo N. Nat Prod Commun 2011;6:1205–15.
[6] Maione F, Cicala C, Musciacco G, De Feo V, Amat AG, Ialenti A, et al. Nat Prod Commun 2013;8:539–44.
[7] Newman DJ, Cragg GM. J Nat Prod 2012;75:311–35.
[8] Maione F, De Feo V, Caiazzo E, De Martino L, Cicala C, Mascolo N. J Ethnopharmacol 2014;155:1236–42.
[9] Chen W, Liu L, Luo Y, Odaka Y, Awate S, Zhou H, et al. Cancer Prev Res 2012;5:778–87.
[10] Feng H, Xiang H, Zhang J, Liu G, Guo N, Wang X, et al. J Biomed Biotechnol 2009;2009:1–8.
[11] Lee DS, Lee SH, Noh JG, Hong SD. Biosci Biotechnol Biochem 1999;63:2236–9.
[12] Zhang J, Zhang K, Gao ZG, Paoletta S, Zhang D, Han GW, et al. Nature 2014;509:115–8.
[13] Trott O, Olson AJ. J Comput Chem 2010;31:455–61.
[14] Bach P, Boström J, Brickmann K, van Giezenb JJJ, Groneberg RD, Harvey DM, et al. Eur J Med Chem 2013;65:360–75.
[15] Jagroop IA, Burnstock G, Mikhailidis DP. Platelets 2003;14:15–20.
[16] Zhang J, Zhang K, Gao ZG, Paoletta S, Zhang D, Han GW, et al. Nature 2014;509:119–22.
[17] Chen X, Guo J, Bao J, Lu J, Wang Y. Med Res Rev 2014;34:768–94.
[18] Kwak HB, Sun HM, Ha H, Kim HN, Lee JH, Kim HH, et al. Eur J Pharmacol 2008;601:30–7.
[19] Schrödinger LLC. New York, NY; 2013.